Self-Consistent Mean Field Theory of Lyotropic AB Star Copolymers

Y.-L. Song and C.-Y. D. Lu
Department of Chemistry, National Taiwan University, Taipei 106, Taiwan.
E-mail: cydlu@ntu.edu.tw

ABSTRACT: Using the self-consistent field theory, we study the lamellar, the hexagonal, and the micellar phases of the A_nB_m miktoarm star copolymer with added solvent. We present an algorithm for the SCFT of block copolymers within a specific class of multiple arms chain architecture, and solve the partition function of the polymer chain in the reciprocal space. By changing the arm number of the solvophilic part B of the polymer, we calculate the common mesophases of A_1B_m star copolymers for several m. We construct numerically the phase diagrams in weak solvent selectivity and try to locate the detailed phase boundary between the three mesophases. The microstructures of the star copolymers are affected by the polymer architecture and the solvent concentration. Because of the highly asymmetric structure for the A_1B_3 and the A_1B_5 star copolymers, these star copolymers do not favor the formation of the lamellar phase. We also found that within the same polymer chain composition, the solubility of copolymers increases as the solvophilic arm number increases.

Keywords: SCFT, star copolymer, polymeric solution, phase diagram

Introduction

Over the last few decades, lyotropic polymers have been widely used in personal care products, drug delivery, and other applications[1]. The industry also needs the more water-soluble polymers to save the cost of organic solvents and the reaction times. Because of the addition of solvents, there are more interaction factors between solvents and copolymers. Various micro-structures have been found. Lyotropic copolymers have become new approaches for preparing nano-materials with delicate, accessible self-assembled morphologies[2]. The amphiphilic property of Lyotropic copolymers is very similar to surfactants'. However, the chain length of the polymers could be hundred times more than the surfactants. So that it is much easier to develop the self-consistent field theory (SCFT) to calculate the copolymer phase diagram than the surfactants. In this paper, SCFT is employed to analyze the phase behavior of lyotropic star copolymers in the systems with weak solvent selectivity.

Theoretical Method

We extend the recent SCFT scheme of Matsen and Schick[3], which was developed to study the polymer phase behavior of melts, to solve the partition function by the spectral method. The solvent molecules are included by the method of Huang[4], where the distribution of solvent molecules is simply related to the solvent potential field w_s through the Boltzmann factor. We consider the co-polymer with *n*-arms of A-blocks jointed with *m*-arms of B-blocks at one junction point. We call such copolymer A_nB_m star copolymer. Each copolymer is composed of N segments, and the A-monomer fraction f. The architecture is shown in Fig. 1.

We assume the same Kuhn length a for both the A- and B-monomers. The total volume of the system is fixed to V. The volume fraction of the copolymer is ϕ. The volume fraction of solvent is $(1-\phi)$. The potential fields are contributed from the densities of A, B, and the solvent S through the Flory-Huggins parameter χ_{IJ}, where I and J are the labels of species. The ς here is the Lagrange multipliers for the volume constraint.

$$\begin{aligned} w_A &= \chi_{AB}N\phi_B + \chi_{AS}N\phi_S + \zeta \\ w_B &= \chi_{AB}N\phi_A + \chi_{BS}N\phi_S + \zeta \\ w_S &= \chi_{AS}N\phi_A + \chi_{BS}N\phi_B + \zeta \end{aligned} \tag{1}$$

The total system volume is constrained, so that

$$\phi_A + \phi_B + \phi_S = 1. \tag{2}$$

For an A_nB_m architecture, we define the forward and reverse end-segment distribution functions, $q(\mathbf{r},s)$ and $q^{\dagger}(\mathbf{r},s)$, respectively. The forward end-segment distribution function $q(\mathbf{r},s)$ is proportional to the probability that one chain with sN segments "diffuses" from one of the beginning of A-arm to the position $\mathbf{r}$. $q^{\dagger}(r,s)$ has the similar definition as $q(\mathbf{r},s)$ but diffuses from one of the ends of B-arm to the position $\mathbf{r}$ at the counting length parameter s. The end-segment distribution functions q and $q^{\dagger}$ are related to the linear chain propagator G under the potential field $w(\mathbf{r},s)$. The expression of G is

$$G(\mathbf{r}_i,s_i;\mathbf{r}_f,s_f) \equiv \int_{\mathbf{r}_i}^{\mathbf{r}_f} D[\mathbf{r}_\alpha]P[\mathbf{r}_\alpha;s_i,s_f]\exp\left\{-\int_{s_i}^{s_f} ds \times\left[\gamma(s)w_A(\mathbf{r}_\alpha(s)) + (1-\gamma(s))w_B(\mathbf{r}_\alpha(s))\right]\right\} \tag{3}$$

where the path integral is carried out over all paths of the chain from the position $\mathbf{r}_i$ at the counting length parameter s_i to the position $\mathbf{r}_f$ at s_f. γ is equal to 1 when s is located in the A side and 0 otherwise. All paths from s_i to s_f are weighted by the normal distribution function $P[\mathbf{r}_\alpha;s_i,s_f]$.

We summarize the above definition by writing $q(\mathbf{r},s)$ in terms of the single chain propagator $G(\mathbf{r}_i,s_i;\mathbf{r}_f,s_f)$,

$$q(\mathbf{r},s) = \begin{cases} \int D\mathbf{r}_0 G(\mathbf{r}_0,s_0\ ;\ \mathbf{r},s) & \text{for } 0<s<s_1 \\ \int D\mathbf{r}_1 G(\mathbf{r}_1,\ s_1\ ;\ \mathbf{r},\ s)[q(\mathbf{r}_1,\ s_1^-)]^n \times \\ \quad [q^{\dagger}(\mathbf{r}_1,\ s_1^+)]^{m-1} & \text{for } s_1<s<s_2 \end{cases} \tag{4}$$

The boundary conditions for $q(\mathbf{r},s)$ at its free end $s_0 = 0$ and the junction point s_1 are

$$q(\mathbf{r},0)=1 \tag{5}$$

$$q(\mathbf{r},s_1^+)=[q(\mathbf{r}_1,s_1^-)]^n[q^\dagger(\mathbf{r}_1,s_1^+)]^{m-1}, \tag{6}$$

where $q(\mathbf{r},s_1^+)$ is the limit of the function just after the junction point at the B-part.

Using the definition mentioned above, we also have the expression of $q^\dagger(\mathbf{r},s)$,

$$q^\dagger(\mathbf{r},s)=\begin{cases}\int D\mathbf{r}_1 G(\mathbf{r},s\,;\mathbf{r}_1,s_1)[q(\mathbf{r}_1,s_1^-)]^{n-1}\times \\ \quad [q^\dagger(\mathbf{r}_1,s_1^+)]^m & \text{for } 0<s<s_1 \\ \int D\mathbf{r}_2 G(\mathbf{r},s\,;\mathbf{r}_2,s_2) & \text{for } s_1<s<s_2\end{cases} \tag{7}$$

The boundary conditions for $q^\dagger(\mathbf{r},s)$ at its free end s_2 and the junction point s_1 are

$$q^\dagger(\mathbf{r},s_2)=1 \tag{8}$$

$$q^\dagger(\mathbf{r},s_1^-)=[q(\mathbf{r}_1,s_1^-)]^{n-1}[q^\dagger(\mathbf{r}_1,s_1^+)]^m. \tag{9}$$

We've already known that the end-segment distribution function would satisfy the modified diffusion equation[5]. Namely,

$$\frac{\partial q}{\partial s}\equiv\begin{cases}\frac{1}{6}Na^2\nabla^2 q-w_A(\mathbf{r})q\,, & \text{for } 0<s<s_1 \\ \frac{1}{6}Na^2\nabla^2 q-w_B(\mathbf{r})q\,, & \text{for } s_1<s<s_2\end{cases} \tag{10}$$

$$-\frac{\partial q^\dagger}{\partial s}\equiv\begin{cases}\frac{Na^2}{6}\nabla^2 q^\dagger-w_A(\mathbf{r})q^\dagger, & \text{for } 0<s<s_1 \\ \frac{Na^2}{6}\nabla^2 q^\dagger-w_B(\mathbf{r})q^\dagger, & \text{for } s_1<s<s_2\,.\end{cases} \tag{11}$$

We should first solve the partition function at single chain parts, that is, $q(\mathbf{r},s)$ at $0<s<s_1$ and $q^\dagger(\mathbf{r},s)$ at $s_1<s<s_2$, and then use these solutions to determine the boundary conditions expressed at Eq. (6) and (9). Once the value of $q(\mathbf{r},s)$ is known for all s up to s_2, the partition function for the single-copolymer can be evaluated by

$$Q_C=\int d\mathbf{r}q(\mathbf{r},s_2)\,, \tag{12}$$

where all the possible positions of B-ends have been summed.

The solvent molecule distribution is simply related to the solvent potential field w_S via the Boltzmann distribution. The partition function of solvent is

$$Q_S=V^{-1}\int_V \exp\left[\frac{-w_S(\mathbf{r})}{N}\right]d\mathbf{r}\,. \tag{13}$$

For convenience, here we also define an end-segment distribution function for the solvent molecule, $q_S(\mathbf{r},s)$, which satisfies

$$\frac{\partial q_S(\mathbf{r},s)}{\partial s}=-w_S(\mathbf{r},s)q_S(\mathbf{r},s) \tag{14}$$

with the initial condition $q_S(\mathbf{r},s=0)=1$. The partition function of the solvent molecule can be expressed by $q_S(\mathbf{r},s)$,

$$Q_S=V^{-1}\int_V q_S(\mathbf{r},s=\frac{1}{N})d\mathbf{r}\,. \tag{15}$$

The monomer distribution functions can be computed by the end-segment distribution functions,

$$\begin{aligned}\phi_A(\mathbf{r})&=\frac{n\phi}{Q_C}\int_0^{s_1} ds\, q(\mathbf{r},s)\,q^\dagger(\mathbf{r},s) \\ \phi_B(\mathbf{r})&=\frac{m\phi}{Q_C}\int_{s_1}^{s_2} ds\, q(\mathbf{r},s)\,q^\dagger(\mathbf{r},s) \\ \phi_S(\mathbf{r})&=\frac{(1-\phi)}{Q_S}\exp\left[\frac{-w_S(\mathbf{r})}{N}\right]\,.\end{aligned} \tag{16}$$

Now the potential fields can be calculated from the monomer distribution functions by Eq. (1) and (2). This completes the cycle of self-consistent equation. The free energy for one copolymer chain can be expressed by

$$\frac{F}{nk_BT}\equiv-\ln\frac{Q_C}{n}-N\frac{1-\phi}{\phi}\ln\frac{Q_S}{nN\frac{1-\phi}{\phi}}+V^{-1}\int d\mathbf{r}\left[\chi_{AB}N\phi_A\phi_B\right.$$

$$\left.+\chi_{AS}N\phi_A\phi_S+\chi_{BS}N\phi_B\phi_S-w_A\phi_A-w_B\phi_B-w_S\phi_S\right] \tag{17}$$

The phase diagram can be drawn by compared the free energy between the ordered and disordered phases.

Results and Discussion

We compute the free energy for three kinds of copolymers, that is, A_1B_1, A_1B_3 and A_1B_5, to study the effect of copolymer architectures. The system conditions here are all set with $N=200$, $f=0.4$, $\chi_{AS}=0.7$, $\chi_{BS}=0.4$, $\chi_{AB}N=40$. The phase diagrams for these copolymers are depicted in Fig. 2. The result of A_1B_1 phase diagram (Fig. 2.a) is in agreement with our expectation. A sequence lamellar (L) → hexagonally-packed A-formed cylinder (C_A) → A-formed micelle (MC_A) →disorder (D) is observed as copolymer volume fraction ϕ_C decreases. The values of ϕ_C at boundaries between L/C_A, C_A/MC_A, and MC_A/D, are equal to 0.53, 0.28, 0.15, respectively. The qualitative behavior is consistent with the result of Huang[4]. The A_1B_3 and A_1B_5 phase diagrams (Fig. 2.b and 2.c) show the different phase behavior compared to the one of A_1B_1. The phase sequences for the A_1B_3 and A_1B_5 are the same as hexagonally-packed A-formed cylinder (C_A) → A-formed micelle (MC_A) →disorder (D) when ϕ_C decreases. The phase boundaries shift more to the right side as the copolymer arm number increases. Now we examine the free energy of different phases in more detail. The free energy for the A_1B_3 and A_1B_5 copolymers at different phases were depicted in Fig. 3 and 4, respectively. From comparing the free energy between different phases, we find that both the A_1B_3 and the A_1B_5 copolymers do not favor the formation of lamellar phases. The loss of the lamellar stability is caused by the highly asymmetric architectures for the AB_3 and AB_5 star copolymers. The highly asymmetric architectures are caused by two reasons. One is that the intrinsic structure caused by the different arm numbers between the A- and B-sides. The other reason is the larger solvation for the B-side. The solvation for the B-side leads to that the AB_3 and AB_5 have a larger B-head cross-section as the solvent is absorbed. The B-head swells more for the AB_5 star copolymer than that of the AB_3 star copolymer. The highly asymmetry of the solvation structure leads that the phase transition of cylinder to micelle happens earlier in the AB_5 copolymers than that of AB_3. From the melting concentrations of different copolymers and phases shown

at Table 1, we observe that all mesostructures of AB_5 copolymers melt in the highest copolymer concentration in comparison with AB_1 and AB_3. The solubility of the copolymers increases as the solvophilic arm number increases. This trend is also reported from the experiment[6] and the simulation study[7].

Conclusion

We use the SCFT calculation to analyze the phase behavior of A_1B_m star copolymers. We study three mesophases, that is, the lamellar, the hexagonal-packed cylinder, and the micelle, with three kinds of copolymers. From comparing the free energy at different phases, we construct the phase diagram and find that the A_1B_3 and A_1B_5 copolymers do not favor the formation of lamellar phase. This is caused by the highly asymmetry for the A_1B_3 and A_1B_5 copolymers. The highly asymmetry is originated from the intrinsic architecture of copolymers and the larger solvation ability of the B-parts.

References

1. Malmsten, M, in *Amphiphilic Block Copolymers: Self-assembly and Applications,* edited by P. Alexandridis and B. Lindman, Elsevier, Amsterdam, **2000**.
2. Park, M.; Harrison, C.; Chaikin, P. M.; Register, R. A.; Adamson, D. H. *Science* **1997**, *276*, 1401.
3. Matsen, M. W.; Schick, M. *Phys. Rev. Lett.* **1994**, *72*, 2660.
4. Huang, C. I.; Hsueh, H. Y. *Polymer* **2006**, *47*, 6843.
5. de Gennes, P.-G. *Scaling Concepts in Polymer Physics*. Cornell University Press, Ithaca, NJ, **1979**.
6. Tsitsilianiis, C.; Papanagopoulos, D. *Polymer* **1998**, *39*, 6429.
7. Huh, J.; Kim, K. H.; Ahn, C. H.; Joa, W. H. *J. Chem. Phys.* **2004**, *121*, 4998.

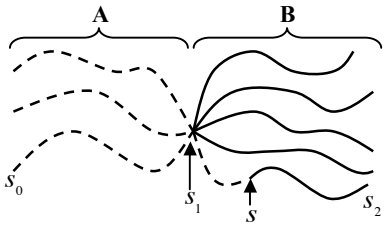

Fig. 1. A schematic diagram of the A_nB_m star co-polymer. The solvophobic A-block contains fN/n segments for each arm. The other solvophilic B-block contains $(1-f)N/m$ segments for each arm. All A-arms are identical, and so are B-arms. We assume the same Kuhn length for both the A- and B-monomers. s is a counting length parameter. At the junction point, $s = s_1 = fN/n$, at the A-start, $s = s_0 = 0$, and at the B-end, $s = s_2 = fN/n+(1-f)N/m$.

Copolymer \ Mesostructure	Micellae $\phi_{c,melt}$	Cylinder $\phi_{c,melt}$	Lamellae $\phi_{c,melt}$
A_1B_1	0.15	0.20	0.20
A_1B_3	0.20	0.25	0.30
A_1B_5	0.25	0.25	0.35

Table 1. The melting concentrations of the different mesostructures for different A_1B_m star copolymers.

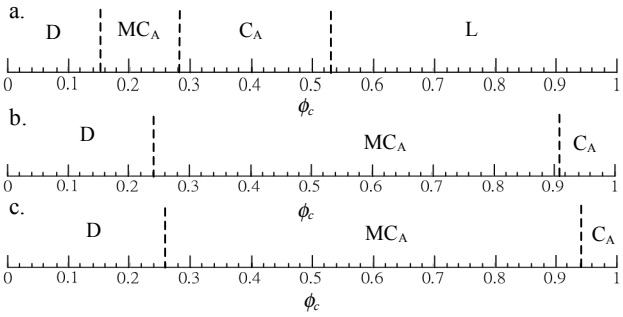

Figure 2. The phase diagram of (a) A_1B_1, (b) A_1B_3, (c) A_1B_5 copolymers in weak selective solvent with $f = 0.4$, $N = 200$, a=0.1, $\chi_{AB}N = 40$, $\chi_{AS} = 0.7$, $\chi_{BS} = 0.4$. D, MC_A, C_A, and L denote the disorder, A-formed micelle, A-formed hexagonal packed cylinder, and lamellar phase, respectively.

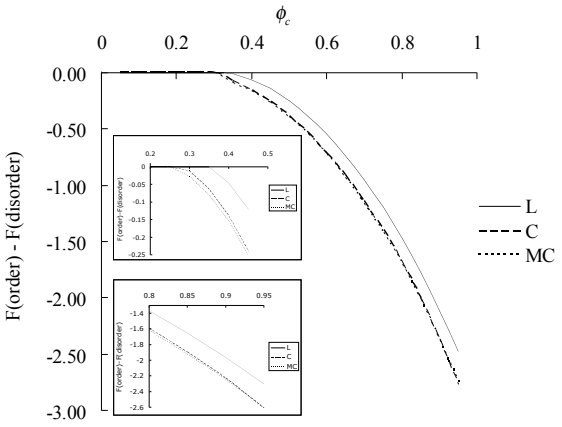

Figure 3. The rescaled free energy of A_1B_3 for three ordered phases.

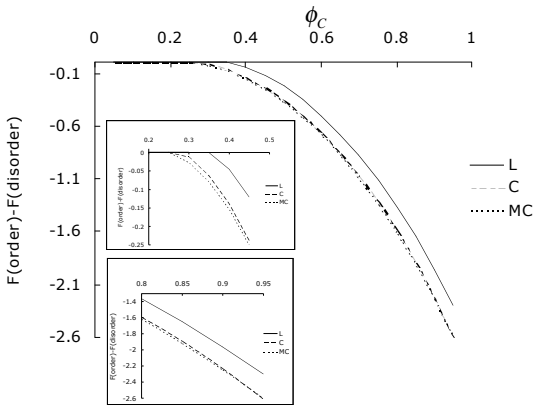

Figure 4. The rescaled free energy of A_1B_5 for three ordered phases.